Multiparameter Structural Optimization of Single-Walled Carbon Nanotube Composites: Toward Record Strength, Stiffness, and Toughness

Bong Sup Shim,[†] Jian Zhu,[†] Edward Jan,[†] Kevin Critchley,[†] Szushen Ho,[†] Paul Podsiadlo,[†] Kai Sun,[‡] and Nicholas A. Kotov[†,§,*]

[†]Department of Chemical Engineering, [‡]Electron Microbeam Analysis Laboratory, and [§]Departments of Materials Science and Biomedical Engineering, University of Michigan, Ann Arbor, Michigan 48109

ABSTRACT Efficient coupling of mechanical properties of SWNTs with the matrix leading to the transfer of unique mechanical properties of SWNTs to the macroscopic composites is a tremendous challenge of today's materials science. The typical mechanical properties of known SWNT composites, such as strength, stiffness, and toughness, are assessed in an introductory survey where we focused on concrete numerical parameters characterizing mechanical properties. Obtaining ideal stress transfer will require fine optimization of nanotube—polymer interface. SWNT nanocomposites were made here by layer-by-layer (LBL) assembly with poly(vinyl alcohol) (PVA), and the first example of optimization in respect to key parameters determining the connectivity at the graphene—polymer interface, namely, degree of SWNT oxidation and cross-linking chemistry, was demonstrated. The resulting SWNT—PVA composites demonstrated tensile strength (σ_{ult}) = 504.5 ± 67.3 MPa, stiffness (E) = 15.6 ± 3.8 GPa, and toughness (K) = 121.2 ± 19.2 J/g with maximum values recorded at σ_{ult} = 600.1 MPa, E = 20.6 GPa, and K = 152.1 J/g. This represents the strongest and stiffest nonfibrous SWNT composites made to date outperforming other bulk composites by 2—10 times. Its high performance is attributed to both high nanotube content and efficient stress transfer. The resulting LBL composite is also one of the toughest in this category of materials and exceeding the toughness of Kevlar by 3-fold. Our observation suggests that the strengthening and toughening mechanism originates from the synergistic combination of high degree of SWNT exfoliation, efficient SWNT—PVA binding, crack surface roughening, and fairly efficient distribution of local stress over the SWNT network. The need for a multiscale approach in designing SWNT composites is advocated.

KEYWORDS: SWNT · nanotube · multilayer assemblies · layer-by-layer assemblies · mechanical properties · nanocomposites · strength · stiffness · toughness

Single-walled carbon nanotubes (SWNTs) are the rolled-up form of graphene sheets, the strongest currently known material.[1] The Young's modulus (stiffness) and ultimate strength of SWNTs are theoretically estimated to be E ~1 TPa, σ_{ult} ~ 300 GPa[2] and experimentally determined to be E ~ 0.64 TPa, σ_{ult} ~ 37 GPa.[1] SWNTs are also extremely tough due to their hollow structures, which allow energy to be absorbed by making inward collapse and plastic deformation.[3] These exceptional mechanical properties of SWNTs, as well as multiwalled carbon nanotubes (MWNTs), have attracted significant research attention for their potential use as reinforcing fillers for polymeric composites. However, macroscale composites made from carbon nanotubes (CNTs) have not yet fully produced the impressive mechanical characteristics possessed by their nanoscale constituents. The individual nanoscale building blocks underperform when they are incorporated into composites due to inefficient stress transfer with the polymer matrix. This represents one of the most challenging problems in materials science, and its resolution has significant implications from both fundamental and practical perspectives.

The road to practical realization of such composites lies through careful structural design of the materials and control of the polymer—nanotube interface. Among other techniques, molecular and nanoscale engineering of different hybrid organic—inorganic materials can be accomplished by using the layer-by-layer assembly (LBL) of composite manufacturing. Compared to the traditional extrusion, mixing, supercritical liquid processing, and other methods of bulk composite preparation, LBL possesses key advantages for nanoscale organization, such as a high degree of structural control, ability to incorporate different nanomaterials in one structure leading to multifunctional composites, and the possibility to produce coatings and free-standing films on 2D and 3D surfaces and topologies. This LBL technique presents another unique advantage in terms of nanoscale mechanics. Intermediate rinsing stages of the LBL process stimulate

*Address correspondence to kotov@umich.edu.

Received for review March 19, 2009 and accepted June 16, 2009.

Published online July 10, 2009.
10.1021/nn9002743 CCC: $40.75

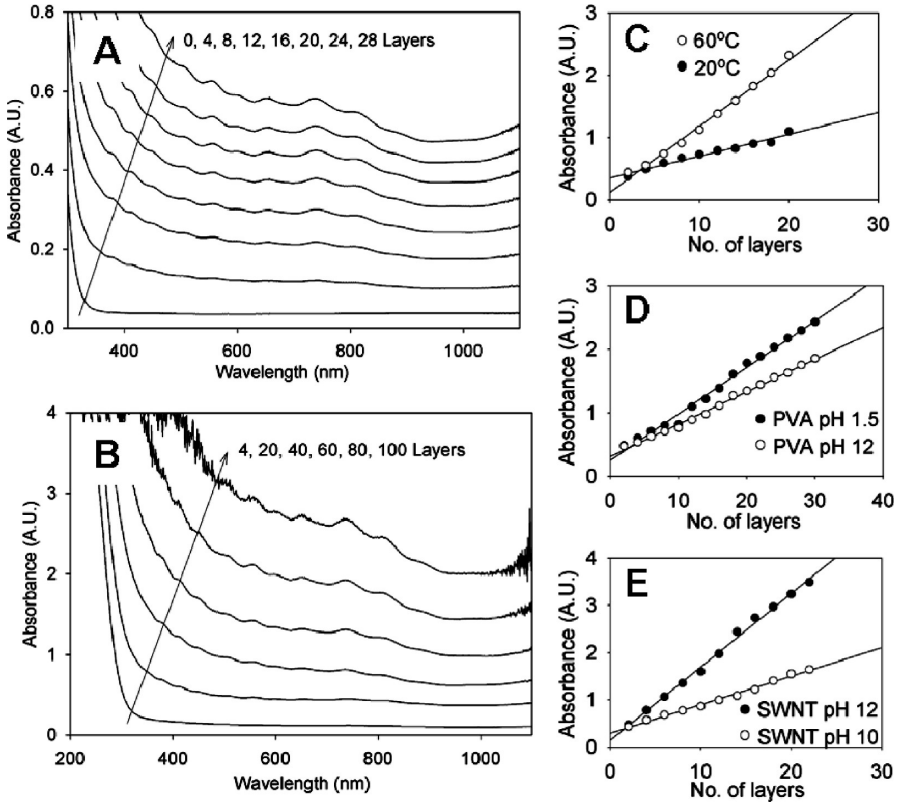

Figure 1. (A,B) UV−vis absorbance spectra of [PVA/SWNT$_{-COOH}$ (15.8)]$_n$ LBL assembly. The values of *n* are indicated in the graphs. (C−E) UV−vis absorbance at 300 nm trend of LBL assembly with various solution conditions: (C) processing temperature, (D) pH of a PVA solution, and (E) pH of a SWNT solution.

efficient interfacial bonding between the components of the composites by removal of polymeric chains loosely attached to SWNTs. The LBL composites have also shown unusually high loadings of SWNTs and excellent homogeneity of the resulting material. Orientation of nanotubes along one direction has been demonstrated during the LBL processing.[4,5] Alignment of reinforcing fillers should help to distribute the stress in the material better than randomly oriented fillers, as was recently demonstrated for clay platelets.[6]

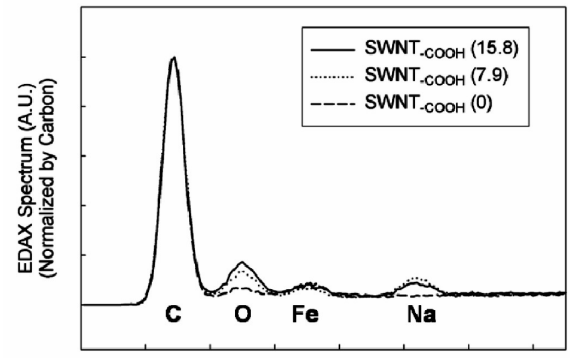

Figure 2. EDAX measurements for SWNT$_{-COOH}$ treated with varied HNO_3 concentrations. Averaged O/C ratio of SWNT$_{-COOH}$(15.8), (7.9), and (0) were 0.23 ± 0.01, 0.199 ± 0.006, and 0.133 ± 0.02, respectively. There are residual amounts of Fe catalysis from SWNT production and Na from acid filtration process.

In this paper, we demonstrate that the utilization of these ideas can lead to substantial improvement in mechanical characteristics that are unmatched by typical bulk composites and can approach mechanical parameters obtained for drawn fibers. Average mechanical properties were found to be $\sigma_{ult} = 504.5 \pm 67.3$ MPa, $E = 15.6 \pm 3.8$ GPa, and $K = 121.2 \pm 19.2$ J/g, and maximum readings as high as $\sigma_{ult} = 600.1$ MPa, $E = 20.6$ GPa, and $K = 152.1$ J/g. The combination of high strength, stiffness, and toughness of these composites puts the SWNT LBL nanocomposite in a unique position among all other bulk and even most fibrous composites reported so far. Overall, the strengthening and toughening mechanisms are likely to be a synergistic multiscale action of intermolecular interactions, improved load transfer by cross-linking, high crack surface roughening, and energy dissipation in microcracks.

Brief Survey of Mechanical Characteristics of Carbon Nanotube Composites. As CNT nanocomposites have been made by a large variety of techniques, it is desirable to extract the principles determining the organization of various nanocomposites from the large amount of available data. As the first step toward this goal, we provide a brief survey of the mechanical parameters reported for nanocomposites produced from different manufacturing methods. In this effort, we avoid extensive discussion of theoretical approaches, which can be found in several recent reviews,[7−9] but focus on simple numerical descriptors. In addition to ultimate strength and stiffness, particular attention is given to toughness (*K*), which, in many cases, we calculated for the reported materials when sufficient data are available in the corresponding publications. In our opinion, *K* is probably the most critical parameter in many applications, ranging from fuel cells[10] to aviation.[11,12] We want to acknowledge that methods of improving *K* in CNT nanocomposite systems are not well-understood[13] and have been achieved in the past mostly by rather accidental discoveries.

CNT−polymer nanocomposite can be divided into two major categories: unidirectional fibers and fairly random bulk composites. There are significant differences in the properties, material design factors, manufacturing approaches, and potential areas of use be-

tween the two categories as well as similarities, such as necessity of strong matrix−nanotube bonding, dense packing of CNT fillers, and the well-known challenge of full exfoliation of CNTs. Furthermore, monodispersity of SWNT structures is receiving growing attention in both directions.[14] The importance of the monodispersity and the exfoliation of SWNTs can be illustrated by a simple example. The cylindrical fillers with 10 and 1 nm in diameter have an order of magnitude difference in the interfacial area between fillers and matrix,[15] which significantly affects the efficiency of load transfer from matrix to nanotubes.[16] Analytical methods used to establish the degree of exfoliation can also be employed to probe the size variations of SWNTs. It includes the indirect optical measurements by UV−vis−NIR spectroscopy (van Hove transitions),[17] Raman spectroscopy,[18] band gap fluorescence microscopy,[19] and direct observations by transmission electron microscopy (TEM) and atomic force microscopy (AFM). A combination of these methods should be applied to characterize nanocomposites.

Unidirectional CNT Nanocomposite Fibers. One of the most obvious and efficient ways to introduce alignment of CNTs is the utilization of shear dynamic forces. Ribbons with a significant degree of alignment were formed by injecting SWNTs dispersed in poly(vinyl alcohol) (PVA) into a vigorously stirred solution. The mechanical properties of the produced fiber were $\sigma_{ult} = 150$ MPa, $E = 15$ GPa, and $K \sim 2$ J/g.[20] Improvements were made with similar solution spinning techniques, yielding fibers of $\sigma_{ult} = 1.8$ GPa and $K = 570$ J/g with 60 wt % of SWNT loading.[21,22] These measurements were rivaled by those of fibers made by the hot drawing approach which produced $\sigma_{ult} = 1.8$ GPa for SWNTs and $\sigma_{ult} = 1.4$ GPa for MWNTs.[23] The toughness measurements for the same materials were reported to be $K = 870$ J/g for SWNTs and $K = 690$ J/g for MWNTs, holding the record for the aligned fiber composites. The high toughness of these CNT fibers was explained by the partial crystallinity of PVA, efficient alignment, and interactions between SWNTs and PVA chains, but no information was disclosed regarding the CNT to PVA ratio and kinds of interactions involved.[24]

Although most solution spinning techniques for fiber production have revealed efficient alignment of SWNTs, very few of them have produced equally impressive performance. We can infer from this observation that specific interactions between CNTs with PVA must have a key role in the mechanical properties. The importance of the matrix is illustrated by SWNT fibers made from sulfuric acid dispersion without polymer matrix.[16] The fibers yielded $\sigma_{ult} = 116$ MPa and $E = 120$ GPa (data were insufficient for calculation of K). Without a polymer binder, the ultimate strength of solution-processed SWNT fibers cited here is an order of magnitude lower than those from polymer-containing fibers.

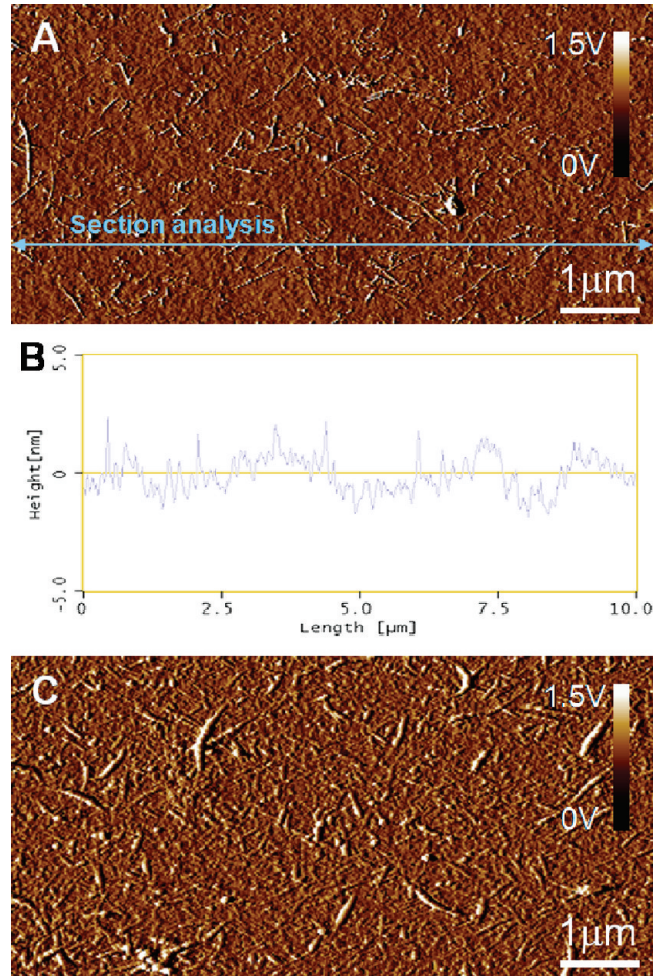

Figure 3. (A) AFM image of [PVA/SWNT$_{-COOH}$(15.8) + PSS]$_1$ and (B) height information of section analysis following blue arrows in (A). (C) AFM image of [PVA/SWNT$_{-COOH}$(15.8) + PSS]$_2$.

Spinning of gels with SWNTs was realized for polyacrylonitrile composites and resulted in 5−10% SWNT loaded fibers with $\sigma_{ult} = 360$ MPa, $E = 16.2$ GPa, and $K \sim 20$.[25] The authors pointed out that the exfoliated state of SWNTs in the solution was not preserved in the fibers as indicated by the disappearance of van Hove transitions.[26] PVA gels can also be spun with SWNTs producing fibers yielding noticeably better performance with $\sigma_{ult} = 1.1$ GPa, $E = 35.8$ GPa, and $K \sim 32$ J/g, although the SWNT content was fairly low—only 3%.[27] Wet spinning of SWNT fiber with poly(*p*-phenylene-2,6-benzoxazole) (PBO) displayed $\sigma_{ult} = 4.2$ GPa, $E = 167$ GPa, and $K \sim 45$ J/g with 10% SWNT content.[28]

Multiwalled carbon nanotubes (MWNTs) can be synthesized in an aligned fashion (*i.e.*, nanotube forest),[29] making dry spinning of CNT fibers possible without an intermediate dispersion stage.[30] Dry spinning was first developed to produce twisted CNT yarns and was later incorporated with polymer infiltration[31] and solvent densification[32] to increase yarn strength. The earlier reports on dry spinning showed density-normalized ultimate strength of $\sigma_{ult}/\rho = \sigma_{ult}{}^{d} = 500$ MPa · cm^3/g.[33] The

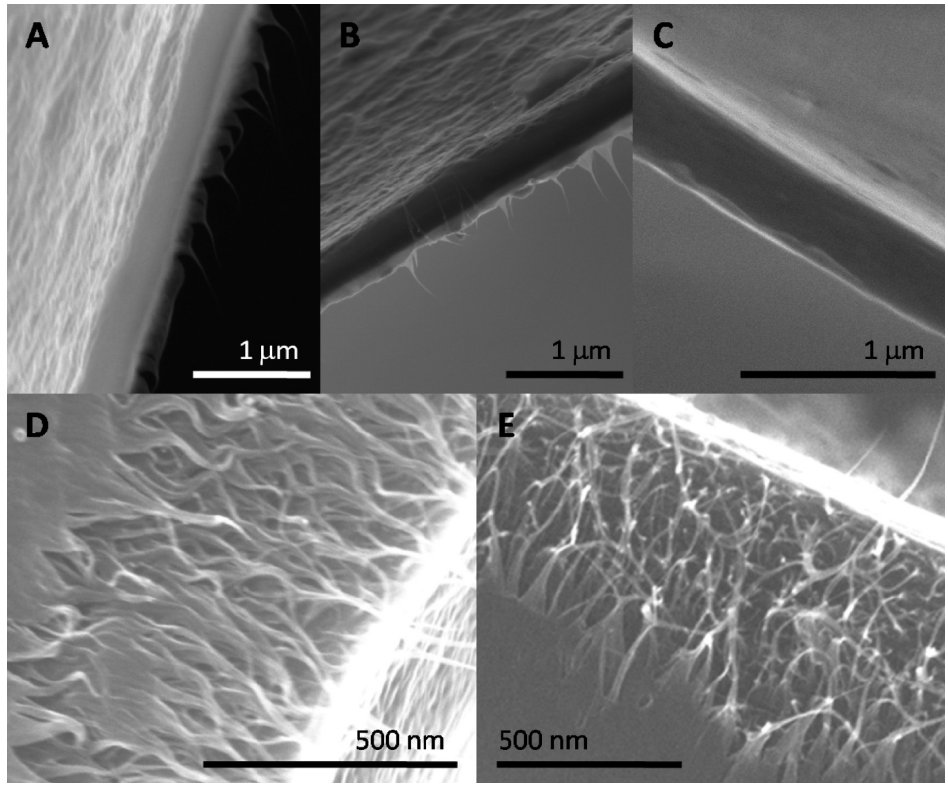

Figure 4. SEM images of LBL film cross sections: (A) [PVA/SWNT$_{-COOH}$(0) + PSS]$_{200}$ with GA treatment, (B) [PVA/SWNT$_{-COOH}$(7.9) + PSS]$_{200}$ with GA treatment, and (C) [PVA/SWNT$_{-COOH}$(15.8) + PSS]$_{200}$ with GA treatment. (D,E) Close-up images of cross sections for [PVA/SWNT$_{-COOH}$(7.9) + PSS]$_{600}$ and [PVA/SWNT$_{-COOH}$(15.8) + PSS]$_{215}$, respectively.

best performance from such a process is an aerogel-type spun fiber showing $\sigma_{ult} = 8.8$ GPa, $E = 357$ GPa, and $K = 121$ J/g.[34] Recently, similarly respectable measurements have been reported for a dry spun fiber having $\sigma_{ult} = 3.3$ GPa, $E = 263$ GPa, and $K = 975$ J/g.[35] Note, however, in this material, most of the energy adsorption took place after the maximum in stress had been reached. Overall, dry spinning improves both strength and stiffness by efficient alignment of intact and long MWNTs, as well as by densification to optimize stress transfer between nanotubes. However, the toughness of matrix-free fibers still suffers compared to those made by solution spinning.

Micro/nanofibrillar sheets have also been made by aligned CNT fibers. The density-normalized strength of transparent sheets woven from CNT yarns was reported to be $\sigma_{ult}^{d} = 175$ MPa $\cdot$ cm^3/g, which exceeds the density-normalized strength of steel, $\sigma_{ult}^{d} \sim 125$ MPa $\cdot$ cm^3/g. For comparison, one can also recall the density-normalized strength of Mylar or Kapton films, $\sigma_{ult}^{d} \sim 160$ MPa $\cdot$ cm^3/g, and aluminum, $\sigma_{ult}^{d} \sim 250$ MPa $\cdot$ cm^3/g.[36] Another unique example is CNT growth on a SiC fabric. The flexural mechanical properties of the SiC−MWNT fabric were $\sigma_{Flexural} = 150$ MPa, $E_{Flexural} = 24$ GPa, and $K_{Flexural} = 30.4$ N mm.[37]

Electrospinning (e-spinning) is also a popular method for preparing nanofiber-based sheets. Polystyrene, polyurethane,[38] Nylon 6,[39] PVA,[40] and polyacrylonitrile[41−43] have been employed as a polymer matrix for electrospun fibers. Polyurethane−SWNT e-spun nanofiber sheets showed $\sigma_{ult} = 15$ MPa, $E = 25$ MPa, and $K \sim 29$ J/g.[38] E-spun polyacrylonitrile composite mats showed a different behavior. With 20% MWNT loading, the e-spun sheets yielded $\sigma_{ult} = 285$ MPa, $E = 14.5$ GPa, and $K \sim 5.4$ J/g.[42]

It must be brought to your attention that most of the CNT-based fibers described so far do not possess mechanical characteristics sufficiently higher than those of commercialized long carbon fibers. For example, the mechanical parameters of the strong Torayca carbon fibers made by Toray Inc. have $\sigma_{ult} = 6.4$ GPa, $E = 294$ GPa, $\varepsilon = 2.2\%$, while the stiff Torayca carbon fibers have $\sigma_{ult} = 3.9$ GPa, $E = 588$ GPa, $\varepsilon = 0.8\%$. Their bulk composites with 60% fiber and epoxy resin claim to achieve $\sigma_{ult} = 3.0$ GPa, $E = 165$ GPa, $\varepsilon = 1.7\%$ and $\sigma_{ult} = 2.0$ GPa, $E = 365$ GPa, and $\varepsilon = 0.6\%$, respectively, for the strong and stiff fibers. These composites are now used industrially in sporting goods, aerospace components, pressure vessels, and so forth.

Homogeneous Bulk Composites. If we compare the data for bulk composites and unidirectional fibers, it is easy to see that mechanical parameters of the bulk composites are significantly lower than those for the fibers, often by an order of magnitude. This is related to several factors. (1) The key structural difference between the two types of composites is the need for nanotubes to stretch and reorganize during the deformation of the bulk nanocomposites, while the stress in the aligned fibers is transferred to

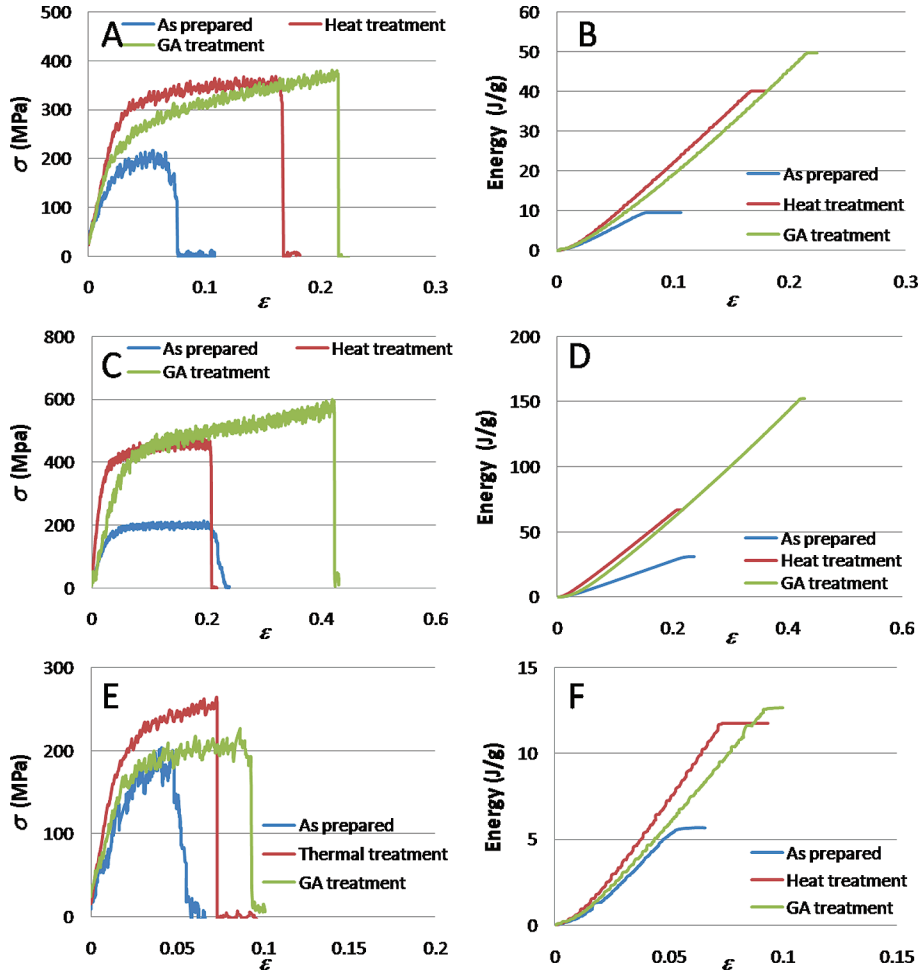

Figure 5. Tension test results of SWNT LBL nanocomposites. (A,C,E) Stress−strain and (B,D,F) toughness−strain curves of (A,B) [PVA/SWNT$_{-COOH}$(15.8) + PSS]$_{200}$, (C,D) [PVA/SWNT$_{-COOH}$(7.9) + PSS]$_{200}$, and (E,F) [PVA/SWNT$_{-COOH}$(0) + PSS]$_{200}$. Additional processing steps of the composites are indicated in the graphs.

the nanoscale "reinforcing bars" in a more efficient manner. (2) Mixtures in kinetically frozen states, such as drawn fibers, have an intrinsically lower degree of phase separation. Segregation of components, even at the nanoscale, creates local defects, which is detrimental for mechanical properties. This process has far greater propensity to take place in thermodynamically equilibrated bulk phases. (3) The CNT loading of aligned fibers is significantly higher than those of the bulk composites in a same volume. We must emphasize that, despite structural advantages, fibrous materials still cannot replace bulk materials for a variety of applications, especially when continuity, flatness, uniformity of heat/electrical/gas transport, or isotropic distribution of stress are required. Furthermore, unidirectional fibers still need secondary macroscale processing to prepregs, fabrics, braids, *etc.*

Keeping these issues in mind, let us survey some of the bulk composites with the best mechanical characteristics reported so far. Typically, more impressive mechanical properties of materials in this class are obtained after chemical cross-linking between the CNTs and the matrix, which can be realized by *in situ* polymerization[44] and direct polymer functionalization of CNTs.[45] It was also proven, theoretically, that cross-linking significantly improves the overall composite strength[46−48] and toughness.[49] These predictions[50] were confirmed by a series of pull-out experiments of CNTs from polymer matrix with various interfaces[51,52] showing that more efficient load transfer to fibers takes place after cross-linking. One representative example is an SWNT−Nylon 6 composite fiber with $\sigma_{ult} = 109$ MPa, $E = 0.790$ GPa, and $K \sim 146$ J/g.[53] Direct functionalization with polyurethanes also produced bulk composites with $\sigma_{ult} = 45$ MPa, $E = 0.0096$ GPa, and $\sigma_{ult} = 38$ MPa, $E = 0.022$ GPa for mixed and grafted composites, respectively.[54] The strain of these materials was as high as $s = 969\%$ (mixed) and $s = 852\%$ (grafted), which corresponded to toughness of $K \sim 124-167$ J/g. Although the strain of elastomeric materials is usually high, the stiffness of these materials is typically fairly low.[55] Analogous results were also obtained for chlorinated polypropylene: $\sigma_{ult} = 49$ MPa, $E = 0.68$ GPa, $K = 108$ J/g.[56] As expected, the same process for epoxy resins gave even stronger and stiffer materials but with lower toughness: $\sigma_{ult} = 104$ MPa, $E = 2.65$ GPa, $K \sim 3.4$ J/g.[57]

TABLE 1. Comparison Table of Ultimate Tensile Strength (σ_{ult}), Stiffness (E), Toughness (K), Strain (ε), and CNT Loading for LBL Composites and Other Materials

samples (estimated CNT loading)	cross-linkage	σ_{ult} (MPa)	E (GPa)	K (J/g)	ε (%)
[PVA/SWNT$_{-COOH}$(15.8) + PSS] LBL (70%)	GA	391.5 ± 36.8	13.2 ± 2.4	42.8 ± 10.5	18 ± 4
	heat	359.9 ± 41.5	15.1 ± 2.8	41.4 ± 7.4	18 ± 3
		257.2 ± 24.6	11.9 ± 2.5	13.8 ± 3.8	11 ± 1
PVA/SWNT$_{-COOH}$(7.9) + PSS] LBL (60%)	GA	504.5 ± 67.3	15.6 ± 3.8	121.2 ± 19.2	39 ± 3
	heat	452.6 ± 30.1	23.0 ± 2.4	47.9 ± 16.9	16 ± 4
		224.5 ± 15.1	11.6 ± 2.0	26.9 ± 10.5	19 ± 7
[PVA/SWNT$_{-COOH}$(0) + PSS] LBL (47%)	GA	233.4 ± 25.7	11.3 ± 2.0	11.3 ± 5.0	8 ± 3
	heat	262.57 ± 2.1	10.9 ± 0.8	12.8 ± 1.5	8 ± 1
		196.6 ± 30.2	14.2 ± 1.7	5.8 ± 3.8	6 ± 2
[PVA/Clay] LBL[6]	GA	400 ± 40	106 ± 11	~ 0.5	0.3 ± 0.04
PVA[6]		40 ± 4	1.7 ± 0.2	~ 7.7	35 ± 4
high performance CNT fiber[34] **(100%)**		8800	357	121	~8
Kevlar fiber[81]		3600	90	33	5
spider silk[81]		1150 ± 200	7.9 ± 1.8	165 ± 30	39
aluminum alloy (7075-T6)		572	71.7	29	11

Cross-linking is a logical approach to improving mechanical characteristics, but recent data suggest that it is not the only answer and probably not the best answer to the question of load transfer improvement.[58] Composites from CNTs with noncovalently attached poly(*p*-phenylene ethynylenes), which are often used in luminescent sensors,[59,60] were demonstrated to yield competitive mechanical properties of σ_{ult} = 250 MPa, E

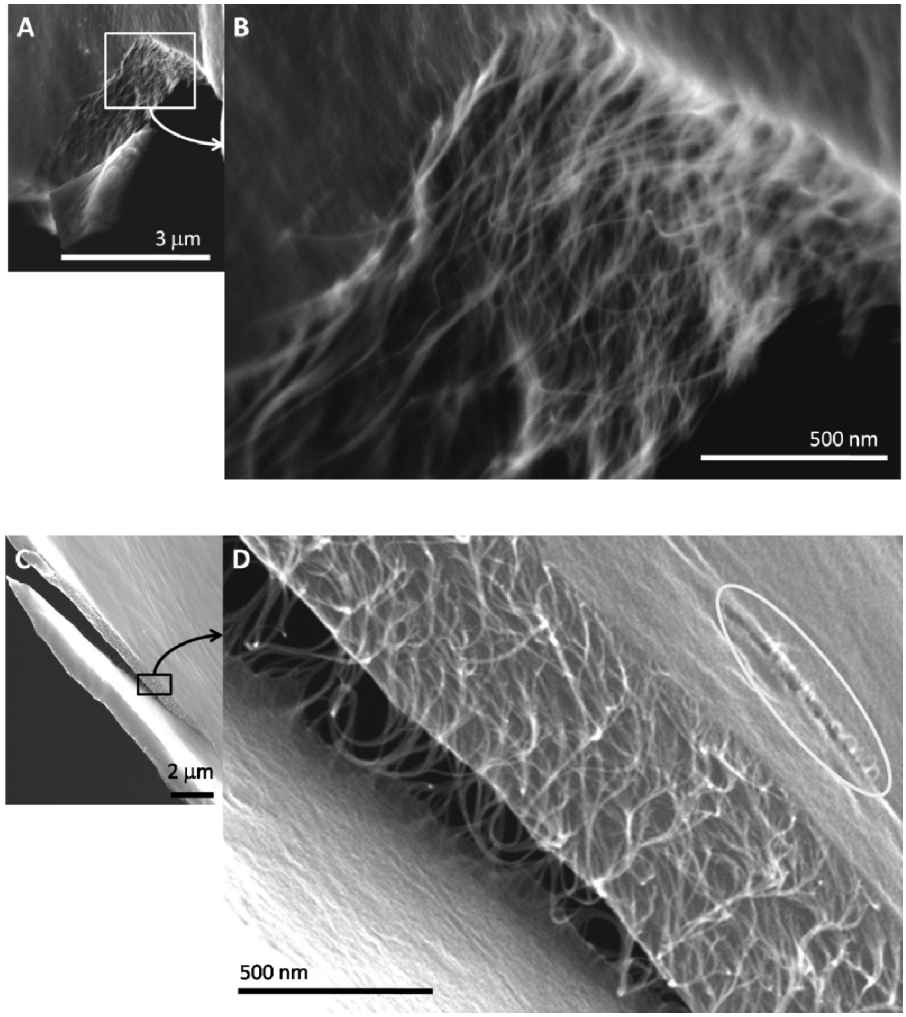

Figure 6. SEM images of torn surfaces of (A,B) a [PVA/SWNT$_{-COOH}$(7.9) + PSS] LBL composite with GA cross-linking and (C,D) a [PVA/SWNT$_{-COOH}$(15.8) + PSS] LBL composite with heat cross-linking.

= 5 GPa, and $K \sim 25$ J/g.[61] Crystallized poly(vinyl alcohol) (PVA) composites with 0.6% MWNT loading were reported to produce $\sigma_{ult} = 348$ MPa, $E = 7.04$ GPa, and $K \sim 6.7$ J/g.[62] Therefore, one may also choose to utilize polymers with strong physical adsorption on the nanotubes. Such polymer chains may order and crystallize around CNTs,[63,64] which can strongly affect the mechanics at the CNT−polymer interface. Toughness was improved 1.7-fold for crystalline PVA reinforced by addition of MWNTs and 4.4-fold for cross-linked PVA−MWNT composites.[62] Note, the CNT content in these composites was fairly low. The same can be noted for other homogeneous bulk composites.[49,65] The toughness of a composite can be greatly improved by chemically grafting CNTs and polymer matrix.[49,66−68] Even 0.5−1% of CNT loading could produce a 3−6 times increase in tensile strength, modulus, strain, and toughness, resulting altogether from a chemical cross-linkage. However, systematic understanding of improvements made by cross-linking is currently fairly empirical and not systematic.

LBL-assembled nanotube materials have more similarities with bulk CNT composites than fibers because the nanotubes in LBL multilayers also undergo substantial restructuring during deformation. With a suboptimal polymer such as poly(ethyleneimine) (PEI), the hybrid composites displayed $\sigma_{ult} = 220$ MPa, $E = 16$ GPa, $K \sim 0.85$ J/g[69] and $\sigma_{ult} = 150$ MPa, $E = 4.5$ GPa, $K \sim 3.7$ J/g[70] for SWNT and MWNT multilayers, respectively. The impressive strength performance with weak polymer compared to other previously mentioned materials is attributed to the uniform CNT dispersion, kinetic thresholds for phase separation, and high loading of CNT fillers. Recently, ordered packing of strong fillers, such as clay nanoplatelets by LBL assembly with PVA and appropriate cross-linking between constituents, showed exceptionally strong and stiff mechanical properties in the resulting composite films.[6]

RESULTS AND DISCUSSION

In this study, SWNTs dispersed in diluted PSS aqueous solutions were LBL-assembled with PVA following procedures described in the Experimental Section. The dissolution in PSS allowed the HiPCo SWNTs to be almost perfectly exfoliated.[71,72] The SWNT colloids were negatively charged due to PSS wrapping and oxidation, while the PVA is neutral under the used conditions of LBL assembly (see Experimental Section). Thus, the traditional understanding of LBL as an alternation of positive/negative components is not completely applicable to these multilayers. The driving force of SWNT−PSS adsorption on PVA is a manifold of fairly weak interactions, which include hydrogen bonding, van der Waals attraction, dipolar electrostatic forces, and hydrophobic interaction.[73] The repetition of LBL cycles resulted in linear film growth, which was identified by UV−vis absorption spectra (Figure 1A,B). The growth rates depended on pH and temperature (Figure 1C,D). After the initial stage of optimization of the layering process, whose description we omitted here for brevity, we chose PVA solution with pH 1.5 and SWNT dispersion with pH 12 as the LBL processing conditions for the preparation of thick free-standing films for mechanical testing. These conditions gave the densest SWNT adsorption per deposition cycle compared to others (Figure 1C−E).

The optical properties of nanomaterials are characterized by discrete excitonic transitions from valence electronic bands to conduction bands. For SWNTs, they are observed in UV−vis−NIR spectra as a series of peaks and shoulders known as van Hove singularities. These peaks and shoulders are not observed from powdered or highly bundled SWNTs because of electronic broadening of energy states, but only from well-separated or exfoliated SWNTs, according to their size and structural distributions. Importantly, for LBL films of SWNTs, the sharp van Hove transitions are observed and do not change as the number of SWNT cycles increases (Figure 1A,B). This indicates that the exfoliation of SWNTs in the solution state can be preserved during LBL assembly and that little electronic coupling with adjacent SWNTs occurs as the film becomes thicker. We would like to point out that the spectral characteristics of SWNT multilayers are in contrast to LBL films made from metal particles in which the plasmon peak shifts strongly with increasing LBL deposition cycles.[74]

To confirm the exfoliated state of adsorbed SWNTs, film topography was observed by tapping mode atomic force microscopy (AFM). The degree of exfoliation of SWNTs was assessed using the height differences obtained in section analysis (Figure 3A,B) as an indicator. Even though few agglomerates were observed, the height of the majority of long strands associated with SWNTs was less than 2 nm, which is indicative of a high degree of exfoliation. Furthermore, few thick strands having cross sections above 2 nm could be due to both localized thick polymer coverage on individual SWNTs and occasional bundles of long and short tubes.

Film samples prepared by LBL were examined in respect to their structure and composition. SEM images of cross sections indicate that the resulting LBL films can be described as dense nonporous materials (Figure 4A−C). The thickness of a 200-bilayer LBL nancomposite ranged between 300 and 400 nm, which corresponds to 1.5−2 nm of adsorption in each deposition cycle. Morphologies reminiscent of combed hair were observed at edges cut by a razor blade (Figure 4D,E). Carbon nanotube contents in the film were varied by changing the surface charge of SWNTs and adsorption of polymer during LBL processing. Overall, the SWNT loading in the LBL films was estimated by TGA to be 47% with $SWNT_{-COOH}(0)$, 60% with $SWNT_{-COOH}(7.9)$, and 72% with $SWNT_{-COOH}(15.8)$ when we compared the tests in air and N_2 environment[72] (see Supporting Information Figure S1). On the basis of the C, O, and S com-

position in the composites, as determined by XPS (Appendix), the estimated content of PSS in the LBL films was 1.1 ± 0, 2.9 ± 2.0, and 2.1 ± 1.2% for SWNT$_{-COOH}$(0), SWNT$_{-COOH}$(7.9), and SWNT$_{-COOH}$(15.8), respectively. Even considering the potential inaccuracy of XPS, the measured amount of PSS in the composites was unexpectedly low. Originally, from 1:2 mass ratio of SWNT/PSS in the dipping solutions, 20−40 times more SWNTs were actually transferred to the solid composites by LBL assembly than PSS. This fact indicates that virtually the only PSS molecules incorporated on the films are those wrapping SWNTs. Free PSS does not adsorb in the LBL process. Also, it is possible that some PSS chains in the solid state are being replaced with PVA and released, driven away by strong interactions between SWNTs and PVA. Under any circumstances, such a process has not been, to the best of our knowledge, reported yet and should significantly affect the mechanical properties.

Because one of the goals of this study was to carry out systematic optimization of the structure of materials in respect to such a complex characteristic as mechanical strength, we had to make a choice in respect to parameters that significantly affect the basic mechanical characteristics. Two principal parameters determining materials' performances were selected: (1) the average density of functional groups on a SWNT; (2) the method of SWNT−matrix cross-linking. Optimizations of other processing factors should, in principle, be done as well, but they probably have a smaller effect on stress transfer at the SWNT−polymer interface.

A greater degree of oxidation makes the interfacial interactions between PVA and SWNTs stronger. However, it also results in the loss of the atomic perfection of SWNTs. Furthermore, creation of functional sites on the SWNT is not uniform. End caps are expected to be oxidized first and side walls later. The average degree of functionalization can be achieved by adjusting acid treatment conditions of SWNTs: HNO_3 concentration and treatment time. We investigated three groups of SWNTs in respect to this parameter: no oxidation (0 M), 7.9 M/1 h, and 15.8 M/2 h (all at room temperature). Indeed, EDAX measurements confirmed that the degree of oxidation varied gradually between these three groups (Figure 2).

Note that the chemistry of the SWNT surface affected not only stress transfer function but also the overall contents of SWNTs in the composites. Significant variations in tensile strength and modulus were observed in respect to the degree of oxidation of SWNTs (Figure 5A,C,E). The changes in the toughness were even stronger. Starting from 7.7 J/g for pure PVA, the toughness of the LBL composites was recorded to be 5.5, 26.9, and 13.8 J/g for SWNT$_{-COOH}$(0), SWNT$_{-COOH}$(7.9), and SWNT$_{-COOH}$(15.8), respectively. These numbers reflect the cumulative effects of simultaneous changes in SWNT contents[71] and stress transfer conditions at the interface between SWNTs and PVA.[62,75] Overall, in comparison with pure PVA, one can improve toughness by as much as 3.5 times.

The two cross-linking methodologies used here were thermal ester bond formation between −COOH in SWNTs and −OH in PVA and glutaraldehyde (GA) treatment, which forms a complex branched matrix by cross-linking PVA chains. We found that the LBL composite with SWNT$_{-COOH}$(7.9) demonstrated the most dramatic effect on mechanical properties from both heat and GA treatments. After cross-linking the [PVA/SWNT$_{-COOH}$(7.9)+PSS]$_{200}$ film, the mechanical properties changed from the original values of σ_{ult} = 224.5 MPa, E = 11.6 GPa, and K = 26.9 J/g to σ_{ult} = 452.6 MPa, E = 23.0 GPa, and K = 47.9 J/g for the heat-treated samples and to σ_{ult} = 504.5 MPa, E = 15.6 GPa, and K = 121.2 J/g for samples after GA treatment. The maximum measurements were recorded at σ_{ult} = 600.1 MPa, E = 20.6 GPa, and K = 152.1 J/g in a GA-treated sample.

As we surveyed in the beginning of the paper, these combinations of high strength, modulus, and toughness are unusually high among all types of homogeneous bulk composites, as well as for some fibers. This should be attributed to simultaneous increase in SWNT loading and significant improvement of stress transfer. The increase of the nanotube content alone cannot lead to great improvements in mechanical properties due to their discrete nature. Bucky paper, which does not display high mechanical properties, can be an ultimate example of this point. It can be compared to the material of the straw or branch house in the classical story of Three Little Pigs. In respect to σ_{ult}, it is easy to see that the prepared materials are stronger than any reported bulk SWNT composites by 2−10 times. They also outperform all the other bulk composites in stiffness (E), sometimes by several orders of magnitude with the closest competitor being E = 7 GPa,[62] which is about 2 times smaller. In respect to toughness (K), the reported data for SWNT composites from polyurethane, $K \sim 124-167$ J/g,[54] are slightly higher than those obtained in optimized LBL samples due to the exceptionally high strain of polyurethanes, which they are very well-known for. However, these composites display much smaller other parameters with σ_{ult} = 38 MPa and E = 0.022 GPa.

While being superior to many fiber composites (see above), LBL SWNT composites do not exceed the best parameters for the drawn SWNT fibers due to the fact that the nanotubes are not aligned: around 10−20 times lower than the high performance CNT fibers in strength and stiffness (Table 1). However, the CNT fibers require secondary processing steps to be used as LBL composites. It is also interesting to compare [PVA/SWNT$_{-COOH}$(7.9) + PSS]$_{200}$ to other materials well-known for their high mechanical properties. As such, the strength of SWNT LBL composites competes with that of aluminum alloys widely used in aviation while exceeding its toughness by about 3-fold. Interesting,

while Kevlar fibers have substantially higher σ_{ult}, their toughness is 3 times smaller than that of [PVA/SWNT$_{-COOH}$(7.9) + PSS]$_{200}$.

It is probably useful to discuss briefly the toughness of composites using a multiscale approach in respect to structural features of the composites at two levels of organization: molecular and nanometer structural features. The combination/optimization of both (with potential addition of micro- and mesoscale structural features) will be the most successful for the further increase of energy dissipation in the materials.

Molecular-scale structural features are represented here by different cross-linking agents, different degrees of oxidation of SWNT, and nanoscale deformations of the constituents (SWNTs in particular). These bonds and interactions are most immediately involved in the stress[49] and sheer transfer[76] at SWNT−polymer interface. Despite the controversial results of the reported effects of cross-linking, mentioned before, one can see in Table 1 that the cross-linked samples demonstrated consistently higher *K* values, as well as the other mechanical parameters, than the non-cross-linked ones. Among them, mechanical parameters for GA-treated LBL assemblies are typically better than those after heat treatment except [PVA/SWNT$_{-COOH}$(0) + PSS]. Obviously, the functional groups on SWNT$_{-COOH}$(0) are not as abundant as for the other nanotube dispersions, and GA has very few "anchor points" to chemically attach them to the polymer. Heat treatment, on the other hand, is likely to result in cross-linking reactions with some double bonds on the graphene surface. Overall, the stress and sheer transfer at the interface between SWNT$_{-COOH}$(0) and PVA/PSS matrix is inferior to that of SWNT$_{-COOH}$(7.9) and SWNT$_{-COOH}$(15.8) despite the fact that some degree of imperfection was introduced to the crystal lattice of carbon atoms.

Different cross-linking techniques result in different density, length, and positioning of covalent bonds. According to previously published data,[77] ester bonds formed by heat treatment are mostly limited to the edges of SWNTs and are short in molecular length. In contrast, GA molecules are inserted between two PVA chains and form ester bridges between −(OH) in PVA and −CHO in GA,[78] producing bonds that are longer and more flexible than the ester cross-links. Hence, the toughness of GA-treated samples is generally better than values of *K* for heat-treated composites (Table 1). Cross-linking makes it possible for the matrix to stretch SWNTs. The fact that the polymer matrix bound to the rigid fillers becomes more rigid as a consequence of strong interfacial interaction with the nanomaterials is likely to be of great help in this respect.[6] The strain transfer to stretchable fillers as a toughening mechanism[79] can be very potent for SWNTs but hard to realize in its ideal case, which leads to dominant failure of nanotubes.

Going up with respect to dimension of structural features, one can also relate toughness to nanometer-scale deformations in the composites. They can be associated with the movement of SWNTs as a whole in the matrix when the stress transfer is not ideal and observed by traditional microscopy techniques and fracture patterns. Fracture behavior resembling that of textiles was observed in the toughest [PVA/SWNT$_{-COOH}$(7.9) + PSS]$_{200}$ LBL film treated with GA using a high-resolution SEM (Figure 6A,B). These densely interwoven SWNT networks evenly and homogeneously distribute the stress over a large volume of the material.

One can also see very strong roughening of the complementary surfaces. This roughened surface results in a greater area of cracks and, hence, requires much greater stress than those of clear-cut surfaces (Figure 6). This might be similar to the toughening mechanism of human cortical bone in transverse breaking.[80] The sample breaks with multiple microcrazing (Figure 6), which can share the stress so that it significantly increases the total capacity of transferred energy as well as the strain, which might be also active in electro-spun SWNT nanofibers.[41]

CONCLUSIONS

In this study, through systematic variation of quantifiable LBL fabrication conditions, we showed that the degree of SWNT oxidation and methods of cross-linking are the primary factors determining the mechanical properties of LBL composites. By tuning of the material structure and the interface bonding, we fabricated a composite material that produced record high mechanical properties not only among nonfibrous composites but also surpassing most fibers drawn from SWNTs and MWNTs. Further improvements of the mechanical properties are certainly possible. However, out-of-the box innovative solutions will be needed for improved stress transfer at the SWNT−polymer interface at molecular scale, nanoscale, and, probably, some special structural features at micro/mesoscale. Otherwise, we see that it will be difficult to realize ideal mechanical coupling between the nanotubes and the matrix. Future directions should include detailed computer simulations of this system to gain fundamental understanding in mechanisms, such as the unusual effect of simultaneously increased strain and toughness upon cross-linking and, potentially, other nanometer-scale mechanics phenomena.

EXPERIMENTAL SECTION

Purified HiPco SWNTs were purchased from Carbon Nanotechnologies Inc. (CNI). In order to incorporate various amounts of functional groups on SWNTs, SWNTs were treated with 15.8 M HNO_3 for 2 h and 7.9 M HNO_3 for 1 h in an ultrasonic bath. These functionalized SWNTs were filtered with PTFE membrane, rinsed with deionized water, and collected as solid powder. We denote SWNT$_{-COOH}$(15.8) and SWNT$_{-COOH}$(7.9), respectively, by the concen-

tration of HNO_3. Nontreated SWNTs were denoted as $SWNT_{-COOH}(0)$. The relative amounts of oxygen incorporated in SWNT−COOH were estimated by EDAX analysis (Figure 2). This powder was re-dispersed in a poly(sodium 4-styrene sulfonate) (PSS, MW 1 000 000, Sigma-Aldrich Co.) solution in an ultrasonic bath for 3 days. The weight ratio of SWNTs and PSS was 1:2, and the concentration of SWNTs was adjusted to 0.05 wt %. Poly(vinyl alcohol) (PVA, MW 195 000, Mowiol 56-98, Kuraray and Fluka) solution was prepared as a counter LBL partner of SWNTs.

LBL assembly was carried out on cleaned glass substrates. First, the glass slide was dipped in a PVA solution (pH 1.5, 0.25 wt %, 20 °C) for 10 min then rinsed in deionized water (pH 5−7) and dried in compressed air. The slide was again dipped in a SWNT dispersion solution (pH 12, 1 wt %, 20 °C) for 10 min then followed by rinsing and drying. This cycle was repeated *n* times, producing a coating with a cumulative structure $[PVA/SWNT_{-COOH}(15.8, 7.9, 0) + PSS]_n$. We used automated LBL deposition robots to minimize the variability of manufacturing parameters.

Bonding of SWNT functional groups to matrix was done by two methods: (1) thermal cross-linking annealing at 220 °C for 10 min; (2) chemical cross-linking by immersion in 5% glutaraldehyde (GA) solution in water for 1 h and subsequent drying in a vacuum. Subsequently, the films were easily peeled off from the substrate by immersing in 1% HF solution.

The mechanical properties of the SWNT composites were obtained by a stretching test in an Instron Q systems model 100 (Test Resources). The free-standing sample strips were cut to 1 ± 0.3 mm of width. The rate of stretching and the initial gap between grips were 0.01 mm/s and 4 ± 1 mm, respectively. For accuracy, all the testing dimensions were directly measured by precision calipers and the measurements were reproduced and averaged 3−5 times.

Scanning electron microscopy (SEM) images were taken by a FEI Nova Nanolab dualbeam FIB and scanning electron microscope. Atomic force microscopy (AFM) imaging was performed with a Nanoscope III atomic force microscope (Digital Instruments/Veeco Metrology Group). X-ray photoelectron spectroscopy (XPS) results were obtained uaing a Kratos Axis Ultra X-ray photoelectron spectrometer. UV−vis absorption measurements were taken using an Agilent 8453E UV−visible spectrometer. Thermogravimetric analysis (TGA) was performed by a PerkinElmer Pyris 1 TGA. Ellipsometric measurements were obtained from an M-44 IR spectroscopic ellipsometer (J. A. Woollam Co., Inc.).

Acknowledgment. The authors want to express much gratitude to the AFOSR program Mechanics of Multifunctional Materials and Microsystems for funding this research. The work was also partially funded by NSF, ONR, DARPA, Dow Chemicals, and Nico Technologies Corp. P. P. thanks the Fannie and John Hertz Foundation for support of his research through a graduate fellowship.

Supporting Information Available: Additional figures. This material is available free of charge *via* the Internet at http://pubs.acs.org.

APPENDIX

TABLE A1. XPS Analysis of SWNT LBL Nanocomposite Films

		amt %			ratio
samples	cross-linkage	C	O	S	C/O
$[PVA/SWNT_{-COOH}(15.8) + PSS]$ LBL film		76.0	23.8	0.2	3.2
	heat	77.3	22.5	0.2	3.4
	GA	77.5	22.3	0.2	3.5
$PVA/SWNT_{-COOH}(7.9) + PSS]$ LBL film		80.3	18.7	0.9	4.3
	heat	77.9	21.8	0.3	3.6
	GA	78.4	21.2	0.3	3.7
$[PVA/SWNT_{-COOH}(0) + PSS]$ LBL film		78.8	20.8	0.3	3.8
	heat	80.8	19.0	0.2	4.3
	GA	80.7	18.7	0.6	4.3

REFERENCES AND NOTES

1. Baughman, R. H.; Zakhidov, A. A.; de Heer, W. A. Carbon Nanotubes—The Route toward Applications. *Science* **2002**, *297*, 787–792.
2. Yu, M. F.; Lourie, O.; Dyer, M. J.; Moloni, K.; Kelly, T. F.; Ruoff, R. S. Strength and Breaking Mechanism of Multiwalled Carbon Nanotubes under Tensile Load. *Science* **2000**, *287*, 637–640.
3. Calvert, P. Nanotube Composites: A Recipe for Strength. *Nature* **1999**, *399*, 210–211.
4. Shim, B. S.; Kotov, N. A. Single-Walled Carbon Nanotube Combing during Layer-by-Layer Assembly: From Random Adsorption to Aligned Composites. *Langmuir* **2005**, *21*, 9381–9385.
5. Shim, B. S.; Podsiadlo, P.; Lilly, D. G.; Agarwal, A.; Lee, J.; Tang, Z.; Ho, S.; Ingle, P.; Paterson, D.; Lu, W.; Kotov, N. A. Nanostructured Thin Films Made by Dewetting Method of Layer-By-Layer Assembly. *Nano Lett.* **2007**, *7*, 3266–3273.
6. Podsiadlo, P.; Kaushik, A. K.; Arruda, E. M.; Waas, A. M.; Shim, B. S.; Xu, J.; Nandivada, H.; Pumplin, B. G.; Lahann, J.; Ramamoorthy, A.; Kotov, N. A. Ultrastrong and Stiff Layered Polymer Nanocomposites. *Science* **2007**, *318*, 80–83.
7. Coleman, J. N.; Khan, U.; Gun'ko, Y. K. Mechanical Reinforcement of Polymers Using Carbon Nanotubes. *Adv. Mater.* **2006**, *18*, 689–706.
8. Coleman, J. N.; Khan, U.; Blau, W. J.; Gun'ko, Y. K. Small but Strong: A Review of the Mechanical Properties of Carbon Nanotube−Polymer Composites. *Carbon* **2006**, *44*, 1624–1652.
9. Moniruzzaman, M.; Winey, K. I. Polymer Nanocomposites Containing Carbon Nanotubes. *Macromolecules* **2006**, *39*, 5194–5205.
10. Steele, B. C. H.; Heinzel, A. Materials for Fuel-Cell Technologies. *Nature* **2001**, *414*, 345–352.
11. Shiflet, G. Materials Science: The More Elements, the Merrier. *Science* **2003**, *300*, 443–444.
12. Jones, R. New Materials, Old Challenges. *Nat. Nanotechnol.* **2007**, *2*, 453–454.
13. Wichmann, M. H. G.; Schulte, K.; Wagner, H. D. On Nanocomposite Toughness. *Compos. Sci. Technol.* **2008**, *68*, 329–331.
14. Hersam, M. C. Progress towards Monodisperse Single-Walled Carbon Nanotubes. *Nat. Nanotechnol.* **2008**, *3*, 387–394.
15. Chae, H. G.; Sreekumar, T. V.; Uchida, T.; Kumar, S. A Comparison of Reinforcement Efficiency of Various Types of Carbon Nanotubes in Polyacrylonitrile Fiber. *Polymer* **2005**, *46*, 10925–10935.
16. Ericson, L. M.; Fan, H.; Peng, H.; Davis, V. A.; Zhou, W.; Sulpizio, J.; Wang, Y.; Booker, R.; Vavro, J.; Guthy, C.; Parra-Vasquez, A. N.; Kim, M. J.; Ramesh, S.; Saini, R. K.; Kittrell, C.; Lavin, G.; Schmidt, H.; Adams, W. W.; Billups, W. E.; Pasquali, M.; Hwang, W. F.; Hauge, R. H.; Fischer, J. E.; Smalley, R. E. Macroscopic, Neat, Single-Walled Carbon Nanotube Fibers. *Science* **2004**, *305*, 1447–1450.
17. Zhang, X.; Liu, T.; Sreekumar, T. V.; Kumar, S.; Moore, V. C.; Hauge, R. H.; Smalley, R. E. Polyvinyl Alcohol/SWNT Composite Film. *Nano Lett.* **2003**, *3*, 1285–1288.
18. Heller, D. A.; Barone, P. W.; Swanson, J. P.; Mayrhofer, R. M.; Strano, M. S. Using Raman Spectroscopy to Elucidate the Aggregation State of Single-Walled Carbon Nanotubes. *J. Phys. Chem. B* **2004**, *108*, 6905–6909.
19. Graff, R. A.; Swanson, J. P.; Barone, P. W.; Baik, S.; Heller, D. A.; Strano, M. S. Achieving Individual-Nanotube Dispersion at High Loading in Single-Walled Carbon Nanotube Composites. *Adv. Mater.* **2005**, *17*, 980–984.
20. Vigolo, B.; Penicaud, A.; Coulon, C.; Sauder, C.; Pailler, R.; Journet, C.; Bernier, P.; Poulin, P. Macroscopic Fibers and Ribbons of Oriented Carbon Nanotubes. *Science* **2000**, *290*, 1331–1334.
21. Dalton, A. B.; Collins, S.; Munoz, E.; Razal, J. M.; Ebron, V. H.; Ferraris, J. P.; Coleman, J. N.; Kim, B. G.; Baughman, R. H. Super-Tough Carbon-Nanotube Fibres. *Nature* **2003**, *423*, 703.

22. Dalton, A. B.; Collins, S.; Razal, J.; Munoz, E.; Ebron, V. H.; Kim, B. G.; Coleman, J. N.; Ferraris, J. P.; Baughman, R. H. Continuous Carbon Nanotube Composite Fibers: Properties, Potential Applications, and Problems. *J. Mater. Chem.* **2004**, *14*, 1–3.
23. Miaudet, P.; Badaire, S.; Maugey, M.; Derre, A.; Pichot, V.; Launois, P.; Poulin, P.; Zakri, C. Hot-Drawing of Single and Multiwall Carbon Nanotube Fibers for High Toughness and Alignment. *Nano Lett.* **2005**, *5*, 2212–2215.
24. Pichot, V.; Badaire, S.; Albouy, P. A.; Zakri, C.; Poulin, P.; Launois, P. Structural and Mechanical Properties of Single-Wall Carbon Nanotube Fibers. *Phys. Rev. B: Condens. Matter* **2006**, *74*, 245416/1–245416/8.
25. Sreekumar, T. V.; Liu, T.; Min, B. G.; Guo, H.; Kumar, S.; Hauge, R. H.; Smalley, R. E. Polyacrylonitrile Single-Walled Carbon Nanotube Composite Fibers. *Adv. Mater.* **2004**, *16*, 58–61.
26. Chae, H. G.; Minus, M. L.; Kumar, S. Oriented and Exfoliated Single Wall Carbon Nanotubes in Polyacrylonitrile. *Polymer* **2006**, *47*, 3494–3504.
27. Zhang, X.; Liu, T.; Sreekumar, T. V.; Kumar, S.; Hu, X.; Smith, K. Gel Spinning of PVA/SWNT Composite Fiber. *Polymer* **2004**, *45*, 8801–8807.
28. Kumar, S.; Dang, T. D.; Arnold, F. E.; Bhattacharyya, A. R.; Min, B. G.; Zhang, X.; Vaia, R. A.; Park, C.; Adams, W. W.; Hauge, R. H.; Smalley, R. E.; Ramesh, S.; Willis, P. A. Synthesis, Structure, and Properties of PBO/SWNT Composites. *Macromolecules* **2002**, *35*, 9039–9043.
29. Zhu, H. W.; Xu, C. L.; Wu, D. H.; Wei, B. Q.; Vajtai, R.; Ajayan, P. M. Direct Synthesis of Long Single-Walled Carbon Nanotube Strands. *Science* **2002**, *296*, 884–886.
30. Jiang, K.; Li, Q.; Fan, S. Spinning Continuous Carbon Nanotube Yarns. *Nature* **2002**, *419*, 801.
31. Zhang, M.; Atkinson, K. R.; Baughman, R. H. Multifunctional Carbon Nanotube Yarns by Downsizing an Ancient Technology. *Science* **2004**, *306*, 1358–1361.
32. Zhang, X.; Jiang, K.; Feng, C.; Liu, P.; Zhang, L.; Kong, J.; Zhang, T.; Li, Q.; Fan, S. Spinning and Processing Continuous Yarns from 4-in. Wafer Scale Super-Aligned Carbon Nanotube Arrays. *Adv. Mater.* **2006**, *18*, 1505–1510.
33. Li, Y. L.; Kinloch, I. A.; Windle, A. H. Direct Spinning of Carbon Nanotube Fibers from Chemical Vapor Deposition Synthesis. *Science* **2004**, *304*, 276–278.
34. Koziol, K.; Vilatela, J.; Moisala, A.; Motta, M.; Cunniff, P.; Sennett, M.; Windle, A. High-Performance Carbon Nanotube Fiber. *Science* **2007**, *318*, 1892–1895.
35. Zhang, X.; Li, Q.; Holesinger, T. G.; Arendt, P. N.; Huang, J.; Kirven, D.; Clapp, T. G.; DePaula, R. F.; Liao, X.; Zhao, Y.; Zheng, L.; Peterson, D. E.; Zhu, Y. Ultrastrong, Stiff, and Lightweight Carbon-Nanotube Fibers. *Adv. Mater.* **2007**, *19*, 4198–4201.
36. Zhang, M.; Fang, S.; Zakhidov, A. A.; Lee, S. B.; Aliev, A. E.; Williams, C. D.; Atkinson, K. R.; Baughman, R. H. Strong, Transparent, Multifunctional, Carbon Nanotube Sheets. *Science* **2005**, *309*, 1215–1219.
37. Veedu, V. P.; Cao, A.; Li, X.; Ma, K.; Soldano, C.; Kar, S.; Ajayan, P. M.; Ghasemi-Nejhad, M. N. Multifunctional Composites Using Reinforced Laminae with Carbon-Nanotube Forests. *Nat. Mater.* **2006**, *5*, 457–462.
38. Sen, R.; Zhao, B.; Perea, D.; Itkis, M. E.; Hu, H.; Love, J.; Bekyarova, E.; Haddon, R. C. Preparation of Single-Walled Carbon Nanotube Reinforced Polystyrene and Polyurethane Nanofibers and Membranes by Electrospinning. *Nano Lett.* **2004**, *4*, 459–464.
39. Jose, M. V.; Steinert, B. W.; Thomas, V.; Dean, D. R.; Abdalla, M. A.; Price, G.; Janowski, G. M. Morphology and Mechanical Properties of Nylon 6/MWNT Nanofibers. *Polymer* **2007**, *48*, 1096–1104.
40. Blond, D.; Walshe, W.; Young, K.; Blighe, F. M.; Khan, U.; Almecija, D.; Carpenter, L.; McCauley, J.; Blau, W. J.; Coleman, J. N. Strong, Tough, Electrospun Polymer–Nanotube Composite Membranes with Extremely Low Density. *Adv. Funct. Mater.* **2008**, *18*, 2618–2624.
41. Ye, H.; Lam, H.; Titchenal, N.; Gogotsi, Y.; Ko, F. Reinforcement and Rupture Behavior of Carbon Nanotubes–Polymer Nanofibers. *Appl. Phys. Lett.* **2004**, *85*, 1775–1777.
42. Ge, J. J.; Hou, H.; Li, Q.; Graham, M. J.; Greiner, A.; Reneker, D. H.; Harris, F. W.; Cheng, S. Z. D. Assembly of Well-Aligned Multiwalled Carbon Nanotubes in Confined Polyacrylonitrile Environments: Electrospun Composite Nanofiber Sheets. *J. Am. Chem. Soc.* **2004**, *126*, 15754–15761.
43. Hou, H.; Ge, J. J.; Zeng, J.; Li, Q.; Reneker, D. H.; Greiner, A.; Cheng, S. Z. D. Electrospun Polyacrylonitrile Nanofibers Containing a High Concentration of Well-Aligned Multiwall Carbon Nanotubes. *Chem. Mater.* **2005**, *17*, 967–973.
44. Gao, J.; Itkis, M. E.; Yu, A.; Bekyarova, E.; Zhao, B.; Haddon, R. C. Continuous Spinning of a Single-Walled Carbon Nanotube-Nylon Composite Fiber. *J. Am. Chem. Soc.* **2005**, *127*, 3847–3854.
45. Dyke, C. A.; Tour, J. M. Covalent Functionalization of Single-Walled Carbon Nanotubes for Materials Applications. *J. Phys. Chem. A* **2004**, *108*, 11151–11159.
46. Frankland, S. J. V.; Caglar, A.; Brenner, D. W.; Griebel, M. Molecular Simulation of the Influence of Chemical Cross-Links on the Shear Strength of Carbon Nanotube-Polymer Interfaces. *J. Phys. Chem. B* **2002**, *106*, 3046–3048.
47. Garg, A.; Sinnott, S. B. Effect of Chemical Functionalization on the Mechanical Properties of Carbon Nanotubes. *Chem. Phys. Lett.* **1998**, *295*, 273–278.
48. Gustavsson, S.; Rosen, A.; Grennberg, H.; Bolton, K. Computational Studies of Carbon Nanotube–Hydrocarbon Bond Strengths at Nanotube Ends: Effect of Link Heteroatom and Hydrocarbon Structure. *Chem.—Eur. J.* **2004**, *10*, 2223–2227.
49. Moniruzzaman, M.; Chattopadhyay, J.; Billups, W. E.; Winey, K. I. Tuning the Mechanical Properties of SWNT/Nylon 6,10 Composites with Flexible Spacers at the Interface. *Nano Lett.* **2007**, *7*, 1178–1185.
50. Frankland, S. J. V.; Harik, V. M. Analysis of Carbon Nanotube Pull-out from a Polymer Matrix. *Surf. Sci.* **2003**, *525*, L103–L108.
51. Barber, A. H.; Cohen, S. R.; Wagner, H. D. Static and Dynamic Wetting Measurements of Single Carbon Nanotubes. *Phys. Rev. Lett.* **2004**, *92*, 186103/1–186103/4.
52. Barber, A. H.; Cohen, S. R.; Wagner, H. D. Measurement of Carbon Nanotube–Polymer Interfacial Strength. *Appl. Phys. Lett.* **2003**, *82*, 4140–4142.
53. Gao, J.; Zhao, B.; Itkis, M. E.; Bekyarova, E.; Hu, H.; Kranak, V.; Yu, A.; Haddon, R. C. Chemical Engineering of the Single-Walled Carbon Nanotube-Nylon 6 Interface. *J. Am. Chem. Soc.* **2006**, *128*, 7492–7496.
54. Xia, H.; Song, M. Preparation and Characterisation of Polyurethane Grafted Single-Walled Carbon Nanotubes and Derived Polyurethane Nanocomposites. *J. Mater. Chem.* **2006**, *16*, 1843–1851.
55. Zhang, W. D.; Shen, L.; Phang, I. Y.; Liu, T. Carbon Nanotubes Reinforced Nylon-6 Composite Prepared by Simple Melt-Compounding. *Macromolecules* **2004**, *37*, 256–259.
56. Blake, R.; Gun'ko, Y. K.; Coleman, J.; Cadek, M.; Fonseca, A.; Nagy, J. B.; Blau, W. J. A Generic Organometallic Approach toward Ultra-Strong Carbon Nanotube Polymer Composites. *J. Am. Chem. Soc.* **2004**, *126*, 10226–10227.
57. Zhu, J.; Peng, H.; Rodriguez-Macias, F.; Margrave, J. L.; Khabashesku, V. N.; Imam, A. M.; Lozano, K.; Barrera, E. V. Reinforcing Epoxy Polymer Composites Through Covalent Integration of Functionalized Nanotubes. *Adv. Funct. Mater.* **2004**, *14*, 643–648.
58. Friddle, R. W.; Lemieux, M. C.; Cicero, G.; Artyukhin, A. B.; Tsukruk, V. V.; Grossman, J. C.; Galli, G.; Noy, A. Single Functional Group Interactions with Individual Carbon Nanotubes. *Nat. Nanotechnol.* **2007**, *2*, 692–697.
59. McQuade, D. T.; Pullen, A. E.; Swager, T. M. Conjugated Polymer-Based Chemical Sensors. *Chem. Rev.* **2000**, *100*, 2537–2574.

60. Westenhoff, S.; Kotov, N. A. Quantum Dot on a Rope. *J. Am. Chem. Soc.* **2002**, *124*, 2448–2449.
61. Chen, J.; Ramasubramaniam, R.; Xue, C.; Liu, H. A Versatile, Molecular Engineering Approach to Simultaneously Enhanced, Multifunctional Carbon Nanotube−Polymer Composites. *Adv. Funct. Mater.* **2006**, *16*, 114–119.
62. Coleman, J. N.; Cadek, M.; Blake, R.; Nicolosi, V.; Ryan, K. P.; Belton, C.; Fonseca, A.; Nagy, J. B.; Gun'ko, Y. K.; Blau, W. J. High-Performance Nanotube-Reinforced Plastics: Understanding the Mechanism of Strength Increase. *Adv. Funct. Mater.* **2004**, *14*, 791–798.
63. Coleman, J. N.; Cadek, M.; Ryan, K. P.; Fonseca, A.; Nagy, J. B.; Blau, W. J.; Ferreira, M. S. Reinforcement of Polymers with Carbon Nanotubes. The Role of an Ordered Polymer Interfacial Region. Experiment and Modeling. *Polymer* **2006**, *47*, 8556–8561.
64. Ryan, K. P.; Cadek, M.; Nicolosi, V.; Blond, D.; Ruether, M.; Armstrong, G.; Swan, H.; Fonseca, A.; Nagy, J. B.; Maser, W. K.; Blau, W. J.; Coleman, J. N. Carbon Nanotubes for Reinforcement of Plastics? A Case Study with Poly(vinyl alcohol). *Compos. Sci. Technol.* **2007**, *67*, 1640–1649.
65. Bhattacharyya, S.; Salvetat, J. P.; Saboungi, M. L. Reinforcement of Semicrystalline Polymers with Collagen-Modified Single Walled Carbon Nanotubes. *Appl. Phys. Lett.* **2006**, *88*, 3.
66. Shi, J. H.; Yang, B. X.; Pramoda, K. P.; Goh, S. H. Enhancement of the Mechanical Performance of Poly(vinyl chloride) Using Poly(*n*-butyl methacrylate)-Grafted Multi-Walled Carbon Nanotubes. *Nanotechnology* **2007**, *18*, 8.
67. Yang, B. X.; Shi, J. H.; Pramoda, K. P.; Goh, S. H. Enhancement of Stiffness, Strength, Ductility and Toughness of Poly(ethylene oxide) Using Phenoxy-Grafted Multiwalled Carbon Nanotubes. *Nanotechnology* **2007**, *18*, 125606.
68. Wang, M.; Pramoda, K. P.; Goh, S. H. Enhancement of the Mechanical Properties of Poly(styrene-*co*-acrylonitrile) with Poly(methyl methacrylate)-Grafted Multiwalled Carbon Nanotubes. *Polymer* **2005**, *46*, 11510–11516.
69. Mamedov, A. A.; Kotov, N. A.; Prato, M.; Guldi, D. M.; Wicksted, J. P.; Hirsch, A. Molecular Design of Strong Single-Wall Carbon Nanotube/Polyelectrolyte Multilayer Composites. *Nat. Mater.* **2002**, *1*, 190–194.
70. Olek, M.; Ostrander, J.; Jurga, S.; Moehwald, H.; Kotov, N.; Kempa, K.; Giersig, M. Layer-by-Layer Assembled Composites from Multiwall Carbon Nanotubes with Different Morphologies. *Nano Lett.* **2004**, *4*, 1889–1895.
71. O'Connell, M. J.; Boul, P.; Ericson, L. M.; Huffman, C.; Wang, Y.; Haroz, E.; Kuper, C.; Tour, J.; Ausman, K. D.; Smalley, R. E. Reversible Water-Solubilization of Single-Walled Carbon Nanotubes by Polymer Wrapping. *Chem. Phys. Lett.* **2001**, *342*, 265–271.
72. Shim, B. S.; Tang, Z.; Morabito, M. P.; Agarwal, A.; Hong, H.; Kotov, N. A. Integration of Conductivity, Transparency, and Mechanical Strength into Highly Homogeneous Layer-by-Layer Composites of Single-Walled Carbon Nanotubes for Optoelectronics. *Chem. Mater.* **2007**, *19*, 5467–5474.
73. Kotov, N. A. Layer-by-layer Self-Assembly: The Contribution of Hydrophobic Interactions. *Nanostruct. Mater.* **1999**, *12*, 789–796.
74. Malikova, N.; Pastoriza-Santos, I.; Schierhorn, M.; Kotov, N. A.; Liz-Marzan, L. M. Layer-by-Layer Assembled Mixed Spherical and Planar Gold Nanoparticles: Control of Interparticle Interactions. *Langmuir* **2002**, *18*, 3694–3697.
75. Chen, W.; Tao, X. M.; Xue, P.; Cheng, X. Y. Enhanced Mechanical Properties and Morphological Characterizations of Poly(vinyl alcohol)−Carbon Nanotube Composite Films. *Appl. Surf. Sci.* **2005**, *252*, 1404–1409.
76. Wang, T.; Dalton, A. B.; Keddie, J. L. Importance of Molecular Friction in a Soft Polymer−Nanotube Nanocomposite. *Macromolecules* **2008**, *41*, 7656–7661.
77. Kumeta, K.; Nagashima, I.; Matsui, S.; Mizoguchi, K. Crosslinking Reaction of Poly(vinyl alcohol) with Poly(acrylic acid) (PAA) by Heat Treatment: Effect of Neutralization of PAA. *J. Appl. Polym. Sci.* **2003**, *90*, 2420–2427.
78. Mansur, H. S.; Orefice, R. L.; Mansur, A. A. P. Characterization of Poly(vinyl alcohol)/Poly(ethylene glycol) Hydrogels and PVA-Derived Hybrids by Small-Angle X-ray Scattering and FTIR Spectroscopy. *Polymer* **2004**, *45*, 7193–7202.
79. Gojny, F. H.; Wichmann, M. H. G.; Fiedler, B.; Schulte, K. Influence of Different Carbon Nanotubes on the Mechanical Properties of Epoxy Matrix Composites—A Comparative Study. *Compos. Sci. Technol.* **2005**, *65*, 2300–2313.
80. Koester, K. J.; Ager, J. W.; Ritchie, R. O. The True Toughness of Human Cortical Bone Measured with Realistically Short Cracks. *Nat. Mater.* **2008**, *7*, 672–677.
81. Vollrath, F.; Knight, D. P. Liquid Crystalline Spinning of Spider Silk. *Nature* **2001**, *410*, 541–548.